New Journal of Physics
The open access journal for physics

Radiation pressure-assisted acceleration of ions using multi-component foils in high-intensity laser–matter interactions

B Aurand[1,2,3,4,9,10], S Kuschel[1,5], O Jäckel[1,5], C Rödel[1,5], H Y Zhao[6], S Herzer[1,5], A E Paz[1,5], J Bierbach[1,5], J Polz[5], B Elkin[7], G G Paulus[1,5], A Karmakar[4,8], P Gibbon[4,8], T Kuehl[1,2,3,9] and M C Kaluza[1,5]

[1] Helmholtz-Institut Jena, D-07743 Jena, Germany
[2] GSI Helmholtzzentrum für Schwerionenforschung, D-64291 Darmstadt, Germany
[3] Universität Mainz, D-55099 Mainz, Germany
[4] ExtreMe Matter Institut, D-64291 Darmstadt, Germany
[5] Institut für Optik und Quantenelektronik, D-07743 Jena, Germany
[6] Institute of Modern Physics, 73000 Lanzhou, People's Republic of China
[7] Fraunhofer Institut für Grenzflächen- und Bioverfahrenstechnik, D-70569 Stuttgart, Germany
[8] Institute for Advanced Simulation, Forschungszentrum Jülich GmbH, D-52428 Jülich, Germany
E-mail: t.kuehl@gsi.de and bastian.aurand@fysik.lth.se

New Journal of Physics **15** (2013) 033031 (11pp)
Received 3 November 2012
Published 22 March 2013
Online at http://www.njp.org/
doi:10.1088/1367-2630/15/3/033031

Abstract. Experimental results on the acceleration of protons and carbon ions from ultra-thin polymer foils at intensities of up to 6×10^{19} W cm^{-2} are presented revealing quasi-monoenergetic spectral characteristics for different ion species at the same time. For carbon ions and protons, a linear correlation between the cutoff energy and the peak energy is observed when the laser intensity is increased. Particle-in-cell simulations supporting the experimental

[9] Authors to whom any correspondence should be addressed.
[10] Current address: Department of Physics, Lund University, SE-22100 Lund, Sweden.

results imply an ion acceleration mechanism driven by the radiation pressure as predicted for multi-component foils at these intensities.

Contents

1. Introduction

After the first observation of megaelectronvolt (MeV) ions generated during the interaction of high-intensity laser pulses with thin foils [1], laser ion acceleration has attracted a great deal of attention. This all-optical approach capable of generating low-emittance and high-laminarity ion pulses [2] of ultra-short duration [3] holds promise for numerous applications such as hadron therapy [4], the fast ignitor concept for inertial confinement fusion [5] and the time-resolved probing of transient electric and magnetic fields [6]. In most experimental studies on laser ion acceleration so far, the mechanism of target-normal-sheath acceleration (TNSA) [7, 8] has been dominant leading to a thermal distribution with a distinct maximum energy of $E_{\mathrm{cutoff}} = 67\,\mathrm{MeV}$ for protons [9]. However, for many applications, this broad energy spread is a major disadvantage as compared to conventional accelerators. Hence, various alternative approaches based on TNSA have been explored experimentally generating ion pulses with narrow, quasi-monoenergetic features in their spectrum. This can be achieved by confining a multi-species ion source laterally or longitudinally. Lateral confinement can be realized using micro-structured [10] or droplet targets [11, 12]. Longitudinal optimization was shown using layered foils [13]. Moreover, peaked energy spectra have been observed in a staged acceleration scenario [14, 15] or with a laser-driven micro lens [16].

A fundamentally different approach is the acceleration by the pressure exerted by the radiation itself [17], initially discussed in the context of space vehicle propulsion [18]. In this scenario, a high-power laser pulse focussed to the intensity I_{L} onto a target exerts a pressure $p = (1 + R)\, I_{\mathrm{L}}/c$, where R is the reflectivity of the target and c is the speed of light. The radiation pressure created by a laser pulse with $I_{\mathrm{L}} > 10^{19}\,\mathrm{W\,cm^{-2}}$ can lead to the uniform acceleration of a macroscopic target [19]. In this case, all particles reach the same velocity, in contrast to the acceleration by the electric sheath field created by the hot electrons in the TNSA scheme. For moderately relativistic intensities, it is predicted that the use of circular polarization significantly reduces the electron heating and hence suppresses TNSA acceleration, such that radiation pressure acceleration (RPA) becomes the dominant mechanism [20, 21]. Experimentally, even for high-intensity laser pulses, circular polarization can be achieved using a quarter-wave plate or a phase-shifting mirror (PSM) [22, 23]. The advantage of a PSM, which is a fully reflective device to manipulate the phase of two orthogonally polarized linear components of the laser pulse, is the high-damage threshold, as well as the low group-delay-dispersion which is induced. When using PSM, unwanted nonlinear effects affecting the beam profile are negligible. With the

rapid progress in laser technology, this might pave the way towards a considerable simplification of accelerator technology.

A comparison between the pressure generated by the laser radiation and the pressure from the electrostatic charge separation induced in the target of thickness d leads to a balance condition $a_0\sqrt{1+R}\approx\sigma$ [24] between the amplitude of the normalized vector potential $a_0 = \sqrt{I_L\lambda_L^2/1.37\times10^{18}\,\mathrm{W\,cm^{-2}}\,\mu\mathrm{m}^2}$ and the normalized target areal density $\sigma = \pi(n_e/n_c\,d/\lambda_L)$. Here, n_e and λ_L are the electron density and laser wavelength, respectively, and $n_c = 1.1\times10^{21}\,\mathrm{cm^{-3}}[\lambda_L/\mu\,\mathrm{m}]^{-2}$ is the critical density. For $\lambda_L = 800\,\mathrm{nm}$ and focused intensities of a few $10^{19}\,\mathrm{W\,cm^{-2}}$ (equivalent to radiation pressures $p\approx30\,\mathrm{Gbar}$), this corresponds to an optimal thickness d for a solid target ($n_e\approx10^{23}\,\mathrm{cm^{-3}}$) of just a few nanometres. The use of such ultra-thin targets, however, creates a stringent requirement on the laser pulse contrast. The first experiments with 30 fs laser pulses in the RPA-regime revealed quasi-monoenergetic features in the spectra of carbon ions [25] using nm-scale diamond-like carbon (DLC) foils. For significantly longer laser pulses ($\tau_L = 500\,\mathrm{fs}$) irradiating similar targets, a mixed acceleration regime combining RPA in a first step followed by the generation of solitary ion waves was inferred by the Los Alamos National Laboratory (LANL) group [26]. A total of 20 MeV proton beams with 1% energy spread have been produced via hole-boring (HB) with CO_2 lasers in hydrogen gas jets [27]. Most recently, Kar *et al* [28] have reported RPA signatures using the VULCAN laser to accelerate ions from a variety of sub-micrometre, multi-species foil targets, demonstrating an energy scaling consistent with a combined HB/light-sail (LS) theory [29]. Previous numerical simulations [30] indicate that high-Z low-Z target combinations can stabilize the acceleration of the lower-Z components via charge transfer to the low-Z component, suppressing transverse instabilities in the latter. At much higher intensities, similar stabilization can be achieved through the higher mass of the substrate layer [31]. In this paper, we report on radiation-pressure-assisted ion acceleration from multi-component foils at moderate intensities and 30 fs pulse lengths, showing quasi-monoenergetic features of protons and carbon ions at the same time.

2. Setup and experimental results

The experiments were carried out using the Jena Ti:Sapphire laser system (JETI) at the University of Jena, the experimental setup is shown in figure 1. JETI delivers laser pulses with a maximum energy of $E_L = 0.8\,\mathrm{J}$ and a pulse duration of $\tau_L = 27\,\mathrm{fs}$. The peak intensity of the fully amplified laser pulse is preceded by a ns-pedestal generated by amplified spontaneous emission with a relative intensity contrast of 10^{-9} and several short prepulses of the order of 10^{-6} which arrive on a timescale of a few 100 ps. In contrast, the maximum proton energy was achieved with an optimal foil thickness of 100 nm when the target was positioned exactly in the focal plane. For thinner foils, however, the peak proton energy was reduced in the focus, while it could be slightly increased by moving the target out of the focal plane by a few Rayleigh lengths. This indicates that the prepulse in the position of best focus was intense enough to partially destroy the thin foil and deteriorate the ion acceleration. The prepulse contrast was then improved by three orders of magnitude using a single-pass plasma mirror [32]. The suppression of the pre-plasma was verified by measuring the highest proton energy from a 2 nm DLC foil which was positioned exactly in the focal plane again. Hence, use of the plasma mirror sufficiently suppressed the deterioration of the target. However, the total laser pulse energy was then reduced to $E_L = 0.5\,\mathrm{J}$ by losses of the plasma mirror. Note that the effects which are reported below could only be

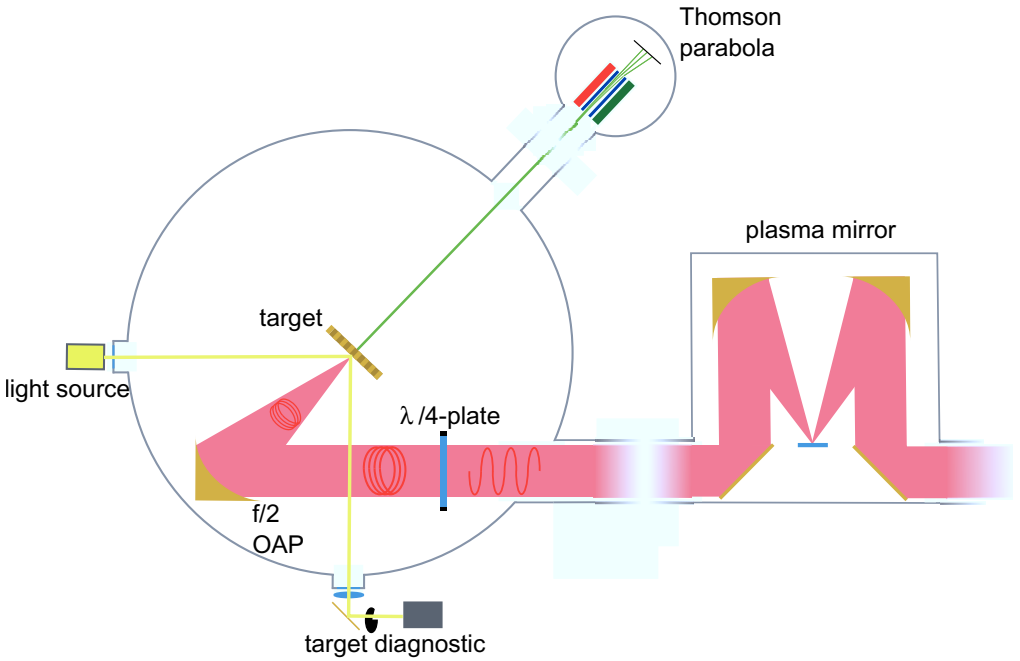

Figure 1. Schematics of the experimental setup: high-intensity laser pulses with variable ellipticity and ultra-high contrast were focused with an $f/2$ off-axis parabolic mirror to an intensity of $6 \times 10^{19}\,\mathrm{W\,cm^{-2}}$ (full-width at half-maximum (FWHM)) onto a nm-thick foil target. The target position and the status of the foil were imaged immediately before each laser pulse. The ion spectra were recorded using a Thomson parabola ion spectrometer.

observed using the plasma mirror delivering laser pulses with a contrast ratio below 10^{-8} until 10 ps before the peak intensity.

A remote-controlled, 70 mm diameter mica quarter-wave plate was used to vary the ellipticity ϵ of the laser polarization achieving values between $0 \leqslant \epsilon \leqslant 0.87$. After that, the pulses were focused with a gold-coated $f/2$ off-axis parabolic mirror onto a foil target of several nm thickness under normal incidence. 30% of the pulse energy was contained within an area of $A_{\mathrm{FWHM}} = 6\,\mu\mathrm{m}^2$ leading to a maximum intensity of $I_{\mathrm{L}} = 6 \times 10^{19}\,\mathrm{W\,cm^{-2}}$ ($a_0 = 5.3$). The ion spectra were recorded in target normal direction by a Thomson parabola covering a solid angle of 2.9×10^{-6} sr. A double-stage micro-channel plate and a phosphor screen were used as a detector which was imaged onto a 12-bit CCD camera. The ion spectrometer was absolutely calibrated with CR39 detectors. In contrast to radiochromic film stacks, this diagnostic guarantees a much higher energy resolution in the sub-MeV per nucleon range. Due to the comparably small acceptance angle, special care was taken when analysing the observed spectral variations, since they might also be caused by variations in the transverse ion beam profile. This will be described below. Both DLC foils with density $\rho = 2.7\,\mathrm{g\,cm^{-3}}$ and thicknesses $2\,\mathrm{nm} \leqslant d \leqslant 100\,\mathrm{nm}$, or parylene foils as multi-component targets $(C_8H_6F_2)_n$ with $\rho = 1.32\,\mathrm{g\,cm^{-3}}$ and thickness of (15 ± 1) or 100 nm were used in the experiment. The parylene foils proved to be easy to handle and comparably resistant against mechanical stress. Parylene is an especially suitable multi-component target in this context due to its high hydrogen content combined with two other atomic species, thus giving a comparatively low density.

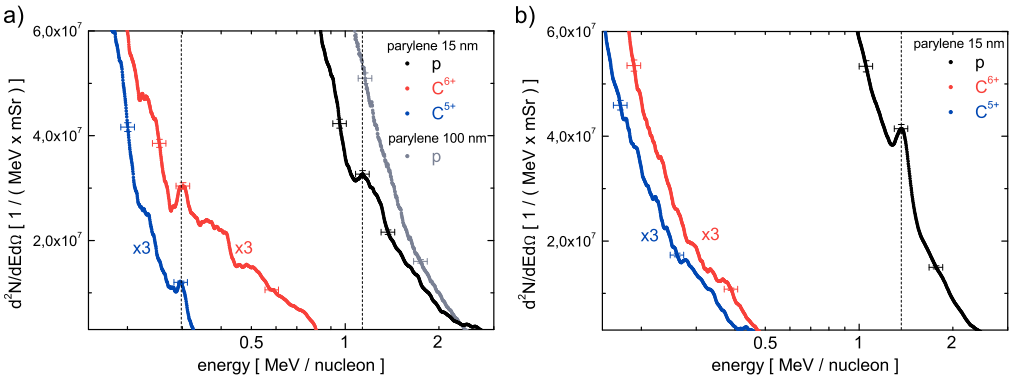

Figure 2. (a) Typical ion energy spectra. The signal height for the carbon ions is multiplied by a factor of 3. Quasi-monoenergetic signatures in the protons and carbon C^{6+} and C^{5+} ion spectra are simultaneously observed on top of a smooth thermal background. A typical energy spectrum obtained with a 100 nm parylene foil irradiated by identical laser parameters is shown for comparison. In this case, no modulation was observed. (b) Spectra from a single shot showing more pronounced modulations in the proton trace, but no distinct features in the other ion species.

For DLC foils, as well as for thicker parylene foils, we mainly observed thermal energy spectra. In the case of 15 nm DLC foils, we observed broad spectra extending up to a cutoff energy for accelerated protons of $E_{\mathrm{cutoff}} = 6.5\,\mathrm{MeV}$ and of $E_{\mathrm{cutoff}} = 0.8\,\mathrm{MeV\,u^{-1}}$ for C^{5+} and C^{6+} ions. Only very few shots showed a modulation on top of this distribution as described in [25]. In contrast, ion spectra from the multi-component parylene foils as shown in figure 2(b) reproducibly exhibited quasi-monoenergetic ion peaks on top of the broad thermal distribution which was present for these targets too. This is consistent with the theoretical predictions by Qiao *et al* [30], which suggest that additional heavier ion species within the polymer foil (in this case fluorine) will lead to a stabilization of the acceleration process. The maximum ion energies were the same as compared to the DLC foil of the same thickness. For our experimental conditions, the energy of the peaks E_{peak} was always lower than the respective cutoff energy (protons: $E_{\mathrm{peak}} = 0.9, \ldots, 2\,\mathrm{MeV}$; carbon ions: $E_{\mathrm{peak}} = 0.3, \ldots, 0.7\,\mathrm{MeV\,u^{-1}}$). Besides the recorded energy spectra showing modulations in protons and carbon ions at the same time, there are a number of shots for which only the proton spectra show a modulation, see figure 2(a). In all these cases, the modulation depth is higher (up to 40%) as compared to shots which show peaks in more than one atomic species.

An intensity scan in the range of $I_{\mathrm{L}} = 0.2, \ldots, 6 \times 10^{19}\,\mathrm{W\,cm^{-2}}$ was performed both by moving the target in longitudinal direction and by reducing the laser pulse energy at the optimum focus position. Peaks in the spectrum of carbon ions and protons were observed simultaneously for a total number of nearly 300 out of around 700 recorded shots. To compare a large number of shots and to account for shot-to-shot fluctuations which can also be caused by variations in the surface flatness of the foil (leading to a different relative position of the foil with respect to the laser focus), we plot the cutoff and peak energies of protons, C^{5+} and C^{6+} ions as a function of the cutoff energy of the C^{6+} ions, which is likely to have a monotonous dependence on the deposited power, see figure 3. A linear dependence with $E_{\mathrm{peak}} = 0.6 \times E_{\mathrm{cutoff}}$

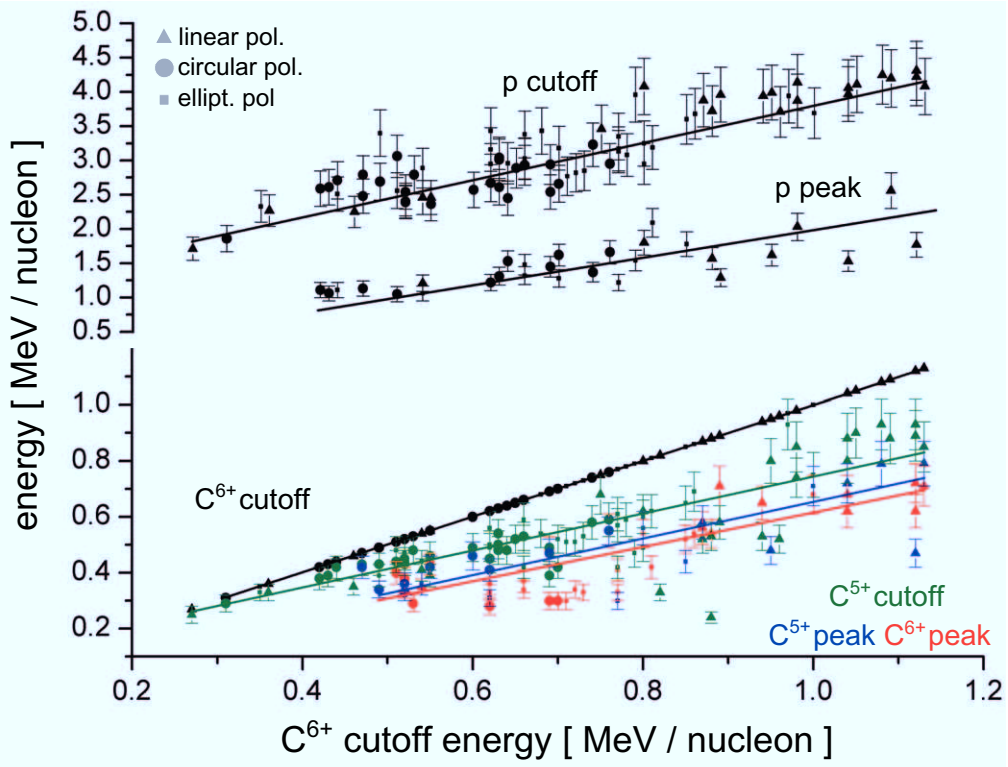

Figure 3. Peak and cutoff energies for protons, C^{5+} and C^{6+} ions, plotted as a function of the C^{6+} cutoff energy for a total number of 111 shot. This presentation also implicitly includes the shot-to-shot variation of the peak intensity. The lowest C^{6+} cutoff energy of 0.27 MeV u^{-1} corresponds to a calculated intensity of 2×10^{18} W cm^{-2}, the highest value of 1.13 MeV u^{-1} to the highest intensity of 6×10^{19} W cm^{-2}. A linear dependence is found for all species. Peak energies for the C^{5+} and C^{6+} ions have the same dependence and are nearly identical. The ellipticity of the laser pulses showed no effect on the appearance of quasi-monoenergetic peaks even at moderate relativistic intensities, but linear polarization led to higher energies compared to circular polarization. The error bars are determined by the resolution of the spectrometer.

was found for each individual ion species. The C^{6+} and C^{5+} peaks reproducibly appeared at nearly the same energy per nucleon, which is indicative for an acceleration driven by radiation pressure, where constant ion velocities are expected. However, the peaks in the proton spectra reproducibly appeared at higher energies. The proton cutoff energy E_{cutoff} is almost 6× higher than the energy corresponding to the same velocity of C^{5+} and C^{6+} ions [33].

The 15 nm parylene foil, satisfying the balance condition $a_0 \approx \sigma$, was used to study the acceleration process relevant for our experimental parameters in more detail. We found that peaks in the ion spectra appeared independent of the polarization state of the incident laser pulse, which is in agreement with the recent results by Kar *et al* [28]. However, the *position* of the peak was affected by the polarization. When using linear polarization, the peaks generally appeared at higher energies as compared to circular polarization, as shown in figure 3. This also was observed in the simulations discussed below, and might hint at a combination of

collective acceleration and TNSA. Using elliptically polarized light, the measured particle energies appeared between the energies for pure linear polarization or the maximum ellipticity which was available in the experiment of $\epsilon_{\max} = 0.87$.

3. Numerical simulations and discussion

To gain more insight into the physical processes prevalent, in our experiment, two-dimensional particle-in-cell (2D-PIC) simulations were carried out using the EPOCH code[11]. Here, the 15 nm parylene foils were modelled with ion number densities $n_C : n_H : n_F = 4 : 3 : 1$ matching their actual composition. They were placed in the centre of a $30 \times 12\,\mu m^2$ large simulation box with grid spacings of $\Delta x = 1$ nm (longitudinal) and $\Delta y = 2.5$ nm (transverse), respectively. For simplicity sake, the ions were assumed to be fully ionized (C^{6+}, H^+, F^{9+}), providing an electron density $n_e = 4 \times 10^{23}\,\mathrm{cm}^{-3} \approx 230 n_c$. Around 6.5 million particles were used to represent all three ion species and the electrons. Circularly or linearly polarized laser pulses with an FWHM spot size of $6\,\mu m^2$, a duration of 27 fs and intensities of $3, \ldots, 6 \times 10^{19}\,\mathrm{W\,cm}^{-2}$ were simulated to irradiate the target under normal incidence.

The numerical results reveal that the acceleration can be described as a two-stage process. During the first stage when the laser pulse is still interacting with the target, initiating a combination of HB and LS acceleration, as described by Kar *et al* [28], the initial HB velocity of the shock front is given approximately by

$$\frac{v_{\mathrm{HB}}}{c} \equiv \beta_0 = \sqrt{\frac{m_e}{m_p}\frac{a_0^2}{\tilde{\rho}}}, \tag{1}$$

where m_e and m_p are the electron and proton masses, respectively, and $\tilde{\rho} = \rho / m_p n_c$ is the dimensionless target mass density. For the highest intensity considered ($a_0 = 5.3$), and a 15 nm parylene foil, we find $\beta_0 \approx 4.4 \times 10^{-3}$. This means that the HB shock front will pass through the foil in 11 fs—well before the end of the pulse, implying that a LS phase will occur for the remainder of the interaction. This is confirmed in figure 4(a), which shows the whole foil already displaced by 100 nm by the time the laser has been reflected.

This situation can, in principle, be compared with the model presented in [28], which predicts a final ion energy of

$$E_{\mathrm{peak}} = \frac{(\mathcal{E} + Z_0)^2}{2(\mathcal{E} + Z_0 + 1)} m_p c^2 \tag{2}$$

with

$$Z_0 = \left(\frac{1+\beta_0}{1-\beta_0}\right)^{1/2} - 1$$

and the normalized fluence

$$\mathcal{E} = \frac{2 I_0 t_L}{\rho d c^2} = 2\frac{m_e}{m_p}\frac{a_0^2 \tau_L}{\tilde{\rho} d/\lambda_L} = 2\pi \frac{Z m_e}{A m_p}\frac{a_0^2 \tau_L}{\sigma}, \tag{3}$$

where $\tau_L = c t_L / \lambda$ (i.e. the number of optical cycles in the pulse). For the above example, we find $\mathcal{E} \approx 0.02$ and $Z_0 \approx \beta_0$, so that $E_{\mathrm{peak}} = 0.27\,\mathrm{MeV\,u}^{-1}$, which is actually consistent with the values seen in figure 2(a) for the C^{5+} and C^{6+} ions. Note that since the exact laser intensities

[11] http://ccpforge.cse.rl.ac.uk/gf/project/epoch

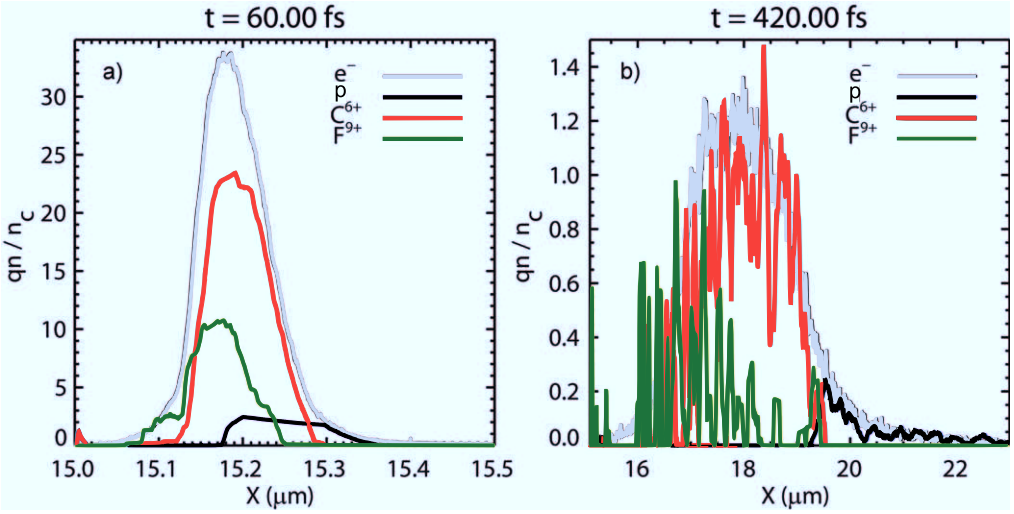

Figure 4. Ion and electron density lineouts along the centre of the simulation box ($y = 6\,\mu$ m), time averaged over three laser cycles: (a) immediately after the laser pulse reflection and (b) towards the end of the simulation.

were not monitored for each shot, a quantitative comparison between the measured peaks and the above model should be treated with caution. On the other hand, the strong scaling $E_{\mathrm{peak}} \sim \mathcal{E}^2$ in this non-relativistic regime means that the expected peak values are sensitive to over or underestimates of I_0.

Nonetheless, support for this correlation can be found in the simulated energy spectra. At this early time (60 fs), the ion bunches correspond to the peaks observed in the spectra of figure 5, which for both C^{6+} and F^{9+} components (with a Z/A of 0.5 and 0.47, respectively) lie at around 0.2 MeV u^{-1}, later becoming washed out during the remainder of the simulation. Again, this result is consistent with the 0.27 MeV u^{-1} predicted by the HB-LS model considering that the HB velocity has been overestimated slightly by neglecting the finite risetime of the pulse. On the other hand, the proton component lies at higher values 0.3–0.5 MeV and doubles by the end of the simulation: features that cannot be accounted for by the above single-slab model.

After the laser pulse has been reflected, a second stage of acceleration starts which is not described by the above model. Here, the electrons are no longer held at the rear side of the foil, but start to oscillate about the (displaced) centre of the ion charge position. This means that the faster-moving protons start to lose their neutralizing electrons in a time-averaged sense, surrendering them back to the stronger positive charge generated by the heavier ions. Note that this situation is almost the reverse of the mixed-ion scenario considered in [30] in which the light protons are able to poach electrons from their heavier counterparts, thereby remaining in a compact bunch while the heavier ions suffer a Coulomb-explosion-driven expansion. In the present experiment, with short pulses at still moderate intensity, the pulse duration is too short to keep the electrons piled up within the proton layer. As a result of this charge imbalance, the leading protons experience an additional electrostatic acceleration, resulting in a final cutoff energy many times higher than the RPA peak energy, see figure 5.

This behaviour is qualitatively similar to the results discussed in [34] or [35], but in our case occurs for much lower intensity and so cannot be compared quantitatively. We therefore conclude that for our experimental conditions, a slight increase in laser intensity results both in

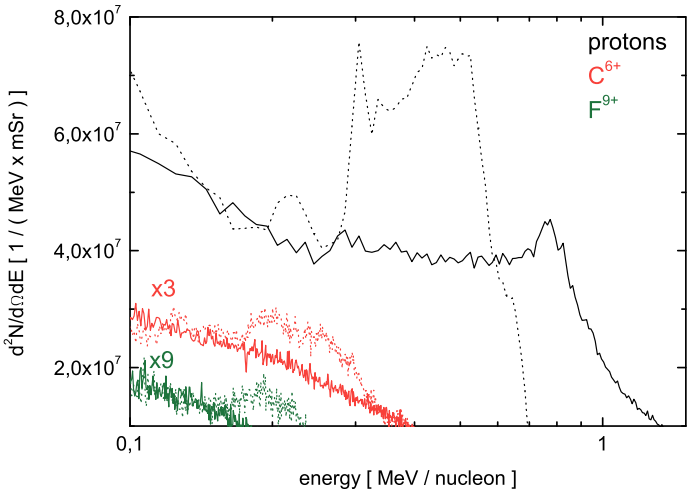

Figure 5. Ion energy spectra simulated for $I_L = 6 \times 10^{19}\,\mathrm{W\,cm^{-2}}$, at $t = 60\,\mathrm{fs}$ (dashed lines) and at $t = 420\,\mathrm{fs}$ (solid), showing a pronounced gap between the proton peak and the high-energy cutoff as observed experimentally. RPA-like peaks are also initially seen in the C and F spectra at $t = 60\,\mathrm{fs}$, but become steadily less pronounced. The signal height of the carbon (fluorine) ions is multiplied by a factor of 3 (9).

a boost of the RPA peak during the first acceleration stage as well as an increase in the cutoff energy by the same amount. This could explain the nearly constant ratio of the peak energy and the cutoff energy that are found in the (implicit) scan of the intensity as seen in figure 3. An additional simulation was carried out using the laser parameters reached in this experiment with linearly polarized light, also leading to a local peak in the proton spectrum. The energy position of this peak and of the resulting cutoff energy of the different ion species is even higher than for circular polarization which is in good agreement with the experimental observation. It is likely that the additional energy is gained by a boost induced by field-induced acceleration (TNSA), which is larger in the case of linearly polarized light than in the case of circularly polarized light. Note that other mechanisms, such as rear-side sheath electrons or the 'directed Coulomb explosion' described in [35] could, in principle, also account for a 'post acceleration' of a lighter ion species, but we see no evidence for either of these processes in the simulations with the laser and target parameters relevant to this experiment. The simulations also indicate that magnetic fields up to a peak amplitude of 4 kT are generated within the foil, decaying to a quarter of this value within 100 fs after the laser has been reflected. These fields should, in principle, lead to a lateral deflection of accelerated ions away from the laser axis, but no evidence of such lateral bunching is found in our simulations which might impact the far-field spectra as in [1]. As mentioned above, an experimental measurement of the lateral distribution was not performed.

In addition to the 15 nm polymer, we also irradiated a 100 nm thick parylene foil with the same laser parameters. In this case, we could not observe any peaked structure in the spectrum similar to those in figure 2(a), as expected from the above model. In this case, the traversal time of the HB shock across the foil is 73 fs—more than twice the pulse length, which means that the LS phase is not reached. The peak energy here can be estimated as $E_f/A = 2m_p c^2 \beta_0^2$, which for these parameters is just $36\,\mathrm{keV\,u^{-1}}$. This may well be reduced by collisional dissipation within the foil and so will be hard to detect in the far field.

4. Conclusion

In conclusion, we have investigated the acceleration of ions from a multi-component nanometre-scale foil target using laser pulses of moderately relativistic intensities. We observed peaked modulations in the energy spectra for several ion species (with differing Z/A) simultaneously. For the carbon ions, the observed peaks in the spectrum are consistent with the fluence/areal density ($a_0^2\tau_L/\rho d$) scaling proposed by Kar *et al* [28], a finding also supported by 2D-PIC simulations, which show that radiation pressure-dominated acceleration takes place as long as the foil is driven by the laser pulse. After this phase, additional acceleration occurs in which the maximum energy of the lightest ion species is further increased by a residual electrostatic interaction. This process does not depend on the laser polarization, but on the maximum electric field of the laser. We have demonstrated that the use of multi-component foils strongly enhances the appearance of quasi-monoenergetic ion acceleration via RPA at 30 fs pulse lengths, and unlike in the (long-pulse) HB regime, leads to a clear separation of heavy and light ion components—an effect that the slab model of [29] does not account for. To this end, our results should improve the understanding of the acceleration processes underlying the acceleration of monoenergetic ion beams with high-intensity lasers.

Acknowledgments

This work was partially supported by the Alliance Program of the Helmholtz Association (HA216/EMMI), by the Thuringian ministry for education, science and culture through EFRE (contract number B715-08006), by the BMBF (contract numbers 03ZIK445 and 03Z1H531), by the DFG (TR18) and by Laserlab Europe. We thank F Ronneberger and B Beleites for their excellent laser support and the GSI target lab. PG acknowledges the useful discussions with L di Lucchio on the physics of the LS mechanism. BA acknowledges the support from HGS-Hire for FAIR, CR from the Carl Zeiss Stiftung. AK and PG gratefully acknowledge the computational resources awarded under project numbers JJSC01 and JZAM04.

References

[1] Clark E L *et al* 2000 *Phys. Rev. Lett.* **85** 1654
[2] Cowan T *et al* 2004 *Phys. Rev. Lett.* **92** 204801
[3] Fuchs J *et al* 2006 *Nature Phys.* **2** 48
[4] Bulanov S V *et al* 2002 *Phys. Lett.* A **299** 240
[5] Roth M *et al* 2001 *Phys. Rev. Lett.* **86** 436
[6] Borghesi M *et al* 2001 *Plasma Phys. Control. Fusion* **43** A267
[7] Wilks S C, Kruer W L, Tabak M and Langdon A B 1992 *Phys. Rev. Lett.* **69** 01383
[8] Mora P 2003 *Phys. Rev. Lett.* **90** 185002
[9] Gaillard S *et al* 2011 *Phys. Plasmas* **18** 56710
[10] Schwoerer H *et al* 2006 *Nature* **439** 445
[11] Ramakrishna B *et al* 2010 *Phys. Plasmas* **17** 083113
[12] Ter-Avetisyan S *et al* 2006 *Phys. Rev. Lett.* **96** 145006
[13] Hegelich B M *et al* 2006 *Nature* **439** 441
[14] Pfotenhauer S M *et al* 2010 *New J. Phys.* **12** 103009
[15] Esirkepov T, Yamagiwa M and Tajima T 2006 *Phys. Rev. Lett.* **96** 105001
[16] Toncian T *et al* 2006 *Science* **312** 410

[17] Veksler V I 1957 *Sov. J. At. Energy* **2** 525
[18] Marx G 1966 *Nature* **21** 22
[19] Wilks S C *et al* 2001 *Phys. Plasmas* **8** 542
[20] Esirkepov T *et al* 2004 *Phys. Rev. Lett.* **92** 175003
[21] Macchi A, Cattani F, Liseykina T V and Cornolti F 2005 *Phys. Rev. Lett.* **94** 165003
[22] Aurand B *et al* 2011 *Opt. Exp.* **19** 17151
[23] Aurand B *et al* 2012 *Rev. Sci. Instrum.* **83** 036104
[24] Yan X Q *et al* 2008 *Phys. Rev. Lett.* **100** 135003
[25] Henig A *et al* 2009 *Phys. Rev. Lett.* **103** 245003
[26] Jung D *et al* 2011 *Phys. Rev. Lett.* **107** 115002
[27] Haberberger D *et al* 2012 *Nature Phys.* **8** 95
[28] Kar S *et al* 2012 *Phys. Rev. Lett.* **109** 185006
[29] Macchi A *et al* 2009 *Phys. Rev. Lett.* **103** 085003
[30] Qiao B *et al* 2010 *Phys. Rev. Lett.* **105** 155002
[31] Yu T P *et al* 2010 *Phys. Rev. Lett.* **105** 065002
[32] Rödel C *et al* 2011 *Appl. Phys.* B **103** 4329
[33] Robinson A P L *et al* 2009 *Plasma Phys. Control. Fusion* **51** 024004
[34] Qiao B *et al* 2012 *Phys. Rev. Lett.* **108** 115002
[35] Bulanov S S *et al* 2008 *Phys. Rev.* E **78** 026412